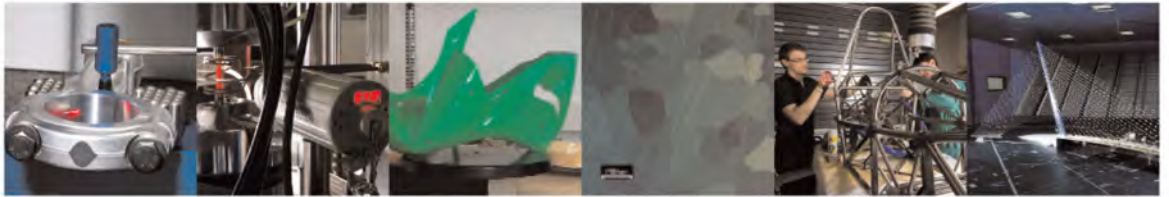




POLITECNICO
MILANO 1863

DIPARTIMENTO DI MECCANICA



Edge States and Topological Pumping in Stiffness Modulated Elastic Plates

Emanuele Riva, Matheus I. N. Rosa and Massimo Ruzzene

This is a post-peer-review, pre-copyedit version of *Edge states and topological pumping in stiffness-modulated elastic plates*, Emanuele Riva, Matheus I. N. Rosa, and Massimo Ruzzene, Phys. Rev. B **101**, 094307. The final authenticated version is available online at: <http://dx.doi.org/10.1103/PhysRevB.101.094307>

©2020 American Physical Society.

This content is provided under [CC BY-NC-ND 4.0](https://creativecommons.org/licenses/by-nc-nd/4.0/) license



Edge States and Topological Pumping in Stiffness Modulated Elastic Plates

Emanuele Riva^a, Matheus I. N. Rosa^b and Massimo Ruzzene^c

^a *Department of Mechanical Engineering, Politecnico di Milano, Italy*

^b *School of Mechanical Engineering, Georgia Institute of Technology, Atlanta GA 30332 and*

^c *Department of Mechanical Engineering, University of Colorado Boulder, Boulder CO 80309*

(Dated: November 11, 2019)

We demonstrate that modulations of the stiffness properties of an elastic plate along a spatial dimension induce edge states spanning non-trivial gaps characterized by integer valued Chern numbers. We also show that topological pumping is induced by smooth variations of the phase of the modulation profile along one spatial dimension, which results in adiabatic edge-to-edge transitions of the edge states. The concept is first illustrated numerically for sinusoidal stiffness modulations, and then experimentally demonstrated in a plate with square-wave thickness profile. The presented numerical and experimental results show how continuous modulations of properties may be exploited in the quest for topological phases of matter. This opens new possibilities for topology-based waveguiding through slow modulations along a second dimension, spatial or temporal.

I. INTRODUCTION

The search for topological phases of matter has reached a mature state with multiple realizations across different physical realms, including quantum¹, electromagnetic^{2,3}, acoustic⁴⁻⁶ and elastic⁷ media. In mechanics, topologically protected wave transport has been demonstrated through analogues to the *Quantum Hall Effect* (QHE)⁸⁻¹⁵, the *Quantum Spin Hall Effect* (QSHE)^{7,16-20} and the *Quantum Valley Hall Effect* (QVHE)²¹⁻²⁴. The rich underlying physics makes these robust waveguiding mechanisms promising for applications in acoustic devices or structural components designed to steer waves or isolate vibrations.

Recently, topological phases have been explored in systems of lower physical dimensions by exploiting synthetic dimensions emerging from the exploration of relevant parameter spaces²⁵⁻²⁸. Notable examples include the observation of edge states, commonly attributed to two-dimensional (2D) QHE systems, in one-dimensional (1D) quantum²⁹, electromagnetic³⁰, acoustic^{31,32} and mechanical³³⁻³⁵ lattices following the Aubry-André-Harper model of interactions^{36,37}. Also, four-dimensional (4D) Quantum Hall phases have been realized using 2D photonic lattices³⁸ and ultracold atoms³⁹, while six-dimensional (6D) phases in 3D systems have been theoretically investigated in^{28,40}. In this context, topological pumping has been pursued in a variety of physical systems, whereby adiabatic transitions of edge states are induced by smooth parameter variations along spatial^{30,34,38,39,41-43} or temporal^{15,44} dimensions. While previous experimental studies demonstrate pumping in photonic lattices and cold atomic gases, a realization using elastic waves is currently missing.

In the quest for topological phases of matter, elastic solids such as thin, elastic plates are promising platforms due to the convenience they offer in terms of manufacturing and testing, and their rich spectral properties which are characterized by a large number of wave modes of distinct polarizations²⁰. At the same time, the abundance of polarizations makes implementing topological

waveguiding in elastic plates a challenging and non trivial development, when compared to acoustic⁴ and electromagnetic^{2,3} counterparts. Towards overcoming these challenges and expanding the range of possibilities for topology-based elastic waveguiding, topological pumping is here experimentally demonstrated for the first time in a continuous elastic plate. The investigations herein leverage prior work on discrete lattices of continuous elastic waveguides³⁴ whereby modulations of physical properties along a spatial dimension were shown to induce edge states spanning non-trivial gaps. Smooth phase variations of the modulation profile along a second spatial dimension induce transitions of the edge modes from being localized at one boundary, to a bulk mode, and finally to a localized mode at the opposite boundary. In here, harmonic stiffness modulation profiles are first investigated to illustrate pumping numerically. Square-wave thickness modulations are then employed in the experimental demonstration of the concept. While the majority of studies has so far focused on discrete lattice systems, our results provide a general strategy to achieve topological pumping through continuous property modulations and open new paths towards exploring higher dimensional topological phases exploiting higher dimensions in continuous systems.

II. ANALYSIS OF EDGE STATES AND TOPOLOGICAL PUMPING IN MODULATED PLATES

We consider elastic plates characterized by a bending stiffness which is periodically modulated along the x direction, *i.e.* $D(x, y) = D(x + \lambda_m, y)$, where λ_m is the modulation wavelength. Two configurations are investigated in this work (Fig. 1). The first one employs a conceptual harmonic stiffness modulation of the form

$$D(x, y) = D_0[1 + a_m \cos(\kappa_m x + \phi(y))] \quad (1)$$

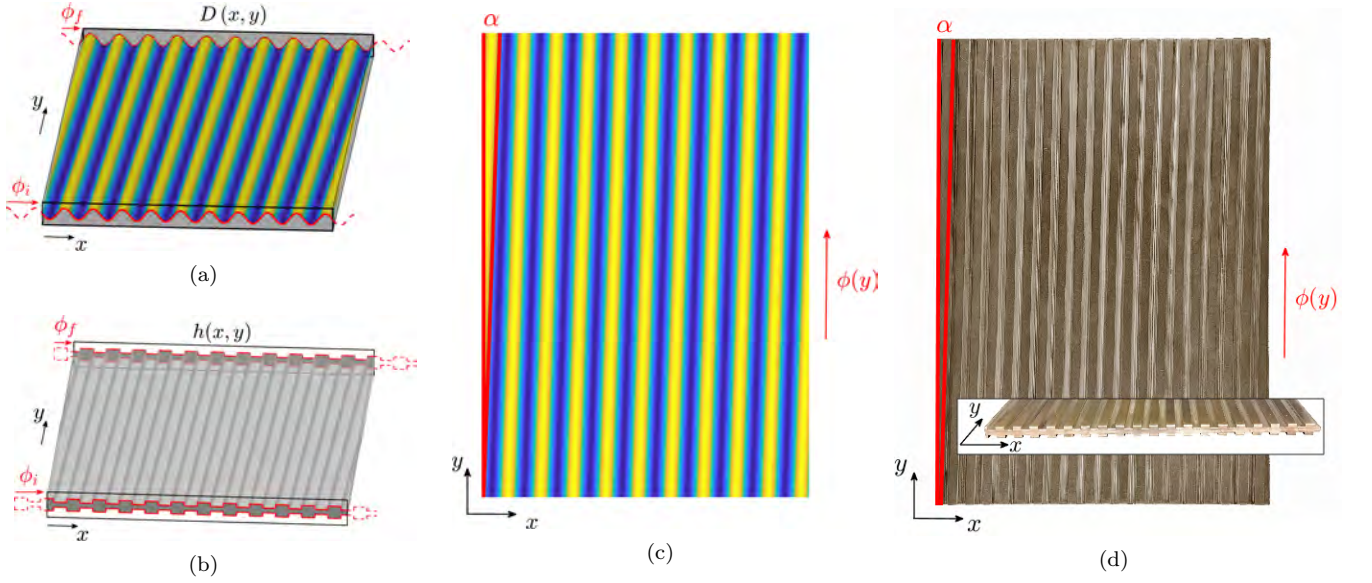


FIG. 1. Stiffness modulations and plate configurations. (a) Plate (shaded gray solid) characterized by a harmonic stiffness modulation $D(x, y) = D_0[1 + a_m \cos(\kappa_m x + \phi(y))]$ (colored surface). The schematic illustrates a linear phase change from ϕ_i to ϕ_f . (b) Schematic of plate with square-wave modulation of thickness $h(x, y) = h_0[1 + a_m \text{sign}(\cos(\kappa_m x + \phi(y)))]$. The phase also varies linearly from ϕ_i to ϕ_f . (c) Top view of modulation in (a) illustrating the shift of the profile characterized by a tilting angle α . (d) Top view and perspective view (inset) of square wave modulated plate employed in experiments. The sample is characterized by parameters $\lambda_m = 1.6$ cm, $h_0 = 4.7$ cm, $a_m = 0.38$, $L_x = 31.2$ cm, $L_y = 43.7$ cm and phase varying linearly from $\phi_i = 0.7\pi$ to $\phi_f = -0.7\pi$.

where $\kappa_m = 2\pi/\lambda_m$, while a_m , and ϕ respectively denote amplitude and phase of the modulation. The phase $\phi(y)$ determines the stiffness value $D(0, y)$ at the left boundary of the plate. If smoothly varied along y , it produces the tilted modulation profile shown in Figs. 1(a,c). This choice follows previous work where sinusoidal modulations define the coupling within continuous waveguides in the context of topological adiabatic pumping³⁴.

The second configuration corresponds to a thickness profile $h(x, y)$ described by a square wave of the form (Fig. 1(b)):

$$h(x, y) = h_0[1 + a_m \text{sign}(\cos(\kappa_m x + \phi(y)))] \quad (2)$$

which produces a periodic modulation of the plate bending stiffness according to the expression $D(x, y) = Eh(x, y)^3/(12(1 - \nu^2))$, where E, ν are respectively the Young's modulus, and the Poisson's ratio of the plate material. This choice is driven by fabrication considerations in the experimental activities of this work.

The effects of the harmonic stiffness modulation (Eqn. (1)) are investigated analytically by considering Kirchhoff-Love's plate theory⁴⁵. According to the theory, the harmonic motion at frequency ω , $w(x, y, \omega)$, in the direction perpendicular to the plate plane x, y is governed by the following equation of motion:

$$[D(w_{,xx} + \nu w_{,yy})]_{,xx} + 2[(1 - \nu)Dw_{,xy}]_{,xy} + [D(w_{,yy} + \nu w_{,xx})]_{,yy} = \omega^2 mw, \quad (3)$$

where $(\cdot)_{,q}$ denotes a partial derivative with respect to q , and $m = \rho h$ is the mass density. We investigate the dispersion properties of the plate $\omega = \omega(\kappa_x, \kappa_y, \phi)$, where the phase modulation ϕ is explicitly denoted as a free parameter. To this end, we impose plane wave solutions $w(x, y) = w(x)e^{j\kappa_y y}$, where $w(x) = \sum_n \hat{w}_n e^{j(\kappa_x + n\kappa_m)x}$, $n = -N, \dots, +N$ reflects the x -wise periodicity of the plate. Application of the Plane Wave Expansion Method (PWEM) (see Supplemental Material (SM)⁴⁶), leads to an eigenvalue problem in the form:

$$\mathbf{K}(\kappa_x, \kappa_y, \phi)\hat{\mathbf{w}} = m\omega^2\hat{\mathbf{w}}, \quad (4)$$

where \mathbf{K} is the $N \times N$ stiffness matrix and $\hat{\mathbf{w}} = \{\hat{w}_{-N}, \dots, \hat{w}_N\}^T$. Solution of the eigenvalue problem in Eqn.(4) yields the dispersion properties, described in terms of eigenvalues ω_i and associate wave modes w_i defined by the components of the eigenvector $\hat{\mathbf{w}}_i$.

We begin our study by evaluating dispersion along x , for assigned values of κ_y . Results for $\kappa_y = 0$, shown in Fig. 2(a), correspond to letting $(\cdot)_{,y} = 0$ in Eqn. (3), which yields an expression akin to the equation governing the transverse motion of 1D elastic Euler Bernoulli beams⁴⁷. In Fig. 2(a), $\mu_x = \kappa_x \lambda_m$, while $\Omega = \omega/\omega_0$ is a non-dimensional frequency, with $\omega_0 = \kappa_m^2 \sqrt{D_0/m}$. The results, obtained for $a_m = 0.8$, effectively correspond to the dispersion characteristics of a family of 1D, decoupled elastic beams characterized by stiffness modulations that differ by the phase parameter ϕ . The dispersion eigenvalues feature two bands separated by a gap that remains

constant with ϕ . Indeed, continuous shifts of the stiffness along x can be interpreted as a translation of the λ_m -periodic unit cell along x , which does not affect the eigenfrequencies. However, these shifts do affect the eigenvectors, as it is revealed by the analysis of the topology of the bands. Such analysis relies on the evaluation of band's Chern number in the $(\mu_x, \phi) \in \mathbb{T}^2 = [0, 2\pi] \times [0, 2\pi]$ space^{34,48}, which is given by

$$C = \frac{1}{2\pi i} \int_{\mathcal{D}} \nabla \times (\mathbf{w}_i^* \cdot \nabla \mathbf{w}_i) d\mathcal{D}, \quad (5)$$

where $\mathcal{D} = \mathbb{T}^2$, $\nabla = (\partial/\partial\mu_x)\mathbf{e}_{\mu_x} + (\partial/\partial\phi)\mathbf{e}_{\phi}$ and $(\cdot)^*$ denotes a complex conjugate. The Chern number is evaluated numerically over a discretized (μ_x, ϕ) space according to the procedure described in⁴⁹, which gives the label assigned to the first band in Fig. 2(a). A label for a gap r is then assigned by computing the algebraic sum of the Chern numbers of the bands below it^{34,48}, *i.e.* $C_g^{(r)} = \sum_{n=1}^r C_n$, which yields $C_g = 1$ for the gap considered in Fig. 2(a). In finite structures, a non-zero gap label signals the presence of topological edge states spanning the associated gap as a result of a parameter sweep. The existence of an edge state as ϕ varies in the $[0, 2\pi]$ range is verified by computing the spectral properties of a plate bounded along the x direction, which are evaluated by constructing an eigenvalue problem similar to that of Eqn. (4), where a solution of the kind $w(x, y) = e^{j\kappa_y y} \sum_n \hat{w}_n \sin(\frac{n\pi x}{L_x})$, $n = 1, \dots, N$ is imposed to satisfy the conditions at the plate x -boundaries, *i.e.* $w(x=0, L_x; y) = w_{,xx}(x=0, L_x; y) = 0$ ⁴⁶. Figure 2(b) shows the modes of a finite plate of length $L_x = 20\lambda_m$ as a function of ϕ , for $\kappa_y = 0$. The modes (black solid lines) belonging to the bulk bands, which are shown for reference as the shaded gray regions, do not vary as a function of ϕ . An additional mode (red line) traversing the gap and varying with ϕ corresponds to a topological edge state localized at either the left or right boundary depending on the value of ϕ , with the right (left) localization of the mode being denoted by the solid (dashed) red line. The transition of the edge state with variations of ϕ is related to the gap label $C_g = 1$. In particular, its absolute value $|C_g| = 1$ indicates that the edge state traverses the gap once for $\phi \in [0, 2\pi]$, while its positive sign relates to a left-to-right transition that occurs when the branch of the edge state touches the upper boundary of the gap at $\phi = \pi$. Representative left-localized (point *I*) and right-localized modes (point *III*) are displayed in Fig. 2(c), along with the mode extending to the bulk in correspondence to the branch touching the bulk band (point *II*). These observations are in agreement with the behavior of edge states and their correspondence to the gap labels in discrete lattices^{34,48}.

Next, we discuss the dispersion properties for values $\kappa_y \neq 0$. These values do not affect the structure of the eigenvalue problem in Eqn. (4), and only introduce a frequency shift. This is illustrated in Fig. 2(d) which displays the dispersion of a modulated plate with $a_m = 0.8$.

The two bands are denoted by the shaded gray volumes, which are spanned for $\mu_x \in [0, \pi]$. Their variation in terms of $\mu_y = \kappa_y \lambda_m$ and ϕ illustrates the presence of a separating gap at frequencies that increase monotonically with μ_y . The modes of a finite plate with $L_x = 20\lambda_m$ populate these bulk bands, here omitted for simplicity, and also include a mode spanning the gap, which is represented by the red surface in the figure. The red lines superimposed at $\mu_y = 0$ illustrate the transition experienced by the edge state as in Fig. 2(b), which now occurs as a function of μ_y along the entire surface of the edge state. To further confirm the topological properties, the Chern number and gap label as previously defined are evaluated as a function of μ_y in discretized $(\mu_x, \phi) \in \mathbb{T}^2 = [0, 2\pi] \times [0, 2\pi]$ spaces, which yields the labels in Fig. 2(d). This result is expected from values $\mu_y \neq 0$ not affecting the dispersion topology.

The transitions of the edge states can be exploited to implement a topological pump that employs an adiabatic (slow) variation of ϕ along a second dimension^{30,34,44,50}. For a finite plate of length L_y , we consider a smooth, linear phase modulation of the kind $\phi(y) = \phi_i \left(1 - \frac{y}{L_y}\right) + \phi_f \frac{y}{L_y}$ (Fig. 1(a)). A top view of a representative harmonic stiffness modulation is displayed in Fig. 1(c), where a positive tilting angle $\alpha = \tan^{-1}(-(\phi_f - \phi_i)/(\kappa_m L_y))$ resulting from a choice with $\phi_i > \phi_f$ is illustrated. We first demonstrate topological pumping numerically by considering a plate with $L_y = 3L_x$ and phase variation with $\phi_i = 0.5\pi$ and $\phi_f = 1.5\pi$. These values cause the edge states to transition from the left boundary to the right boundary. To verify this, we compute the forced response of the plate when harmonically excited by a distributed force per unit area $q(x, y, t) = f(x)\delta(y - y_e)e^{i\omega t}$. The force is applied near the bottom boundary ($y_e = \lambda_m/2$), and has a spatial distribution $f(x)$ that corresponds to the left-localized edge state obtained for $\phi_i = 0.5\pi$ (see Mode *I* in Fig. 1(c)). This favors the excitation of the desired topological mode, while minimizing the contribution from bulk modes co-existing at the same frequency. The response of the plate is evaluated through a Galerkin⁴⁷ approximation of the displacement field $w(x, y)$, similar to that employed to obtain the modes of the finite plate (see details in SM⁴⁶). The response of the plate for an excitation frequency of $\Omega = 10.97$ (Fig. 2(e)) consists of a topological pump whereby energy is transferred from the bottom left boundary to the upper right boundary of the plate via an edge state transition. Additional examples are reported in the Supplementary Material (SM)⁴⁶. The topological pumping results from an adiabatic evolution along the wavenumber branch of the edge state at a given frequency³⁴, which is illustrated for the pump of Fig. 2(e) by considering a cross-section of the dispersion diagram at frequency $\Omega = 10.97$ (blue plane in Fig. 2(d)). The results in Fig. 2(f) are displayed for $\phi \in [0.5\pi, 1.5\pi]$, which is the interval considered for the phase modulation $\phi(y)$. Shaded gray areas correspond to the intersection between the blue plane and the bulk bands (shaded

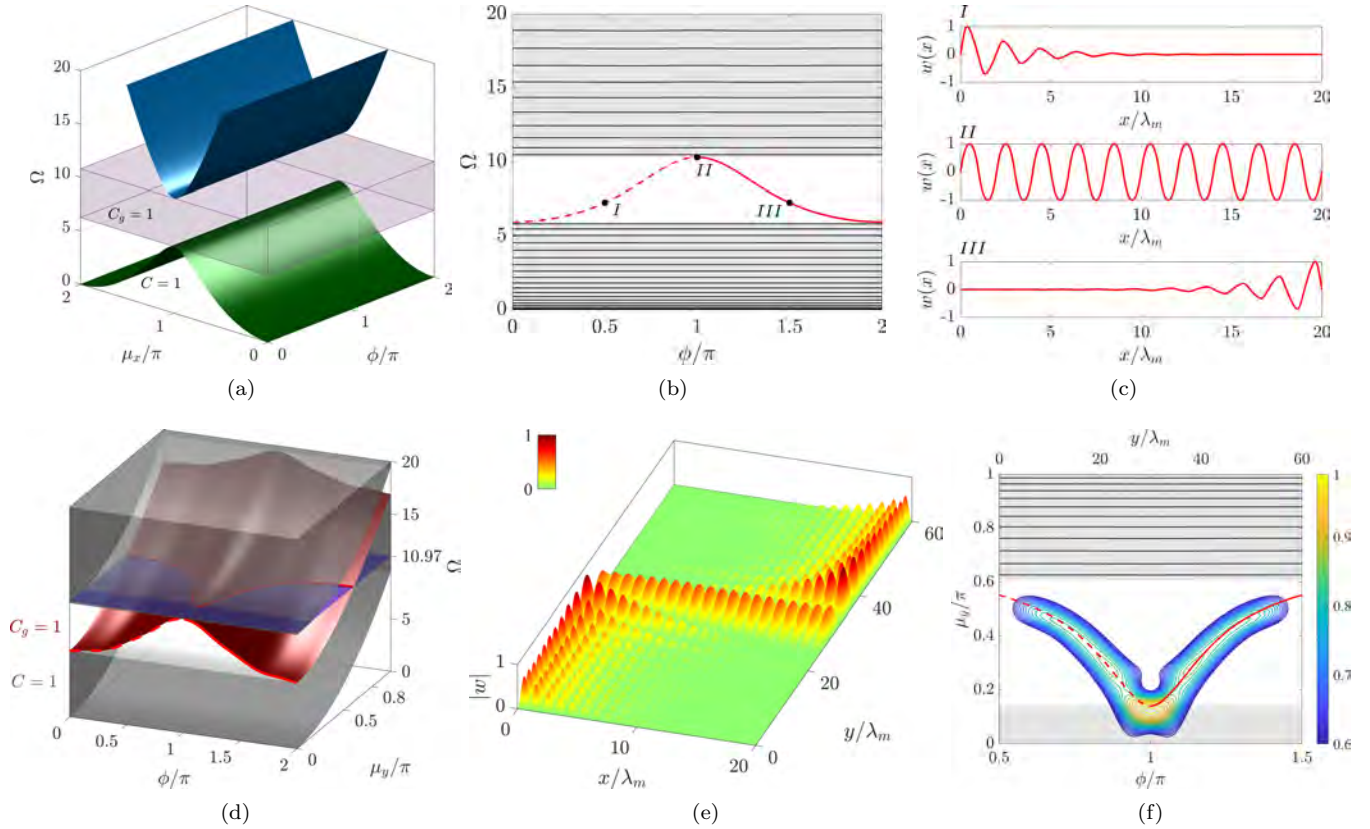


FIG. 2. Dispersion properties and topological pumping for elastic plate with harmonic stiffness modulation $D(x, y) = D_0[1 + a_m \cos(\kappa_m x + \phi(y))]$. (a) Dispersion surfaces $\Omega(\mu_x, \phi)$ for $\mu_y = 0$ showing two bands separated by a gap, with information on Chern numbers and gap label. (b) Frequency spectrum of finite plate with $L_x = 20\lambda_m$ and $\mu_y = 0$ as a function of ϕ : black lines corresponding to finite structure modes are superimposed to the bulk bands (shaded gray regions), while an edge mode (red line) spans the gap. (c) Representative modes for left-localized, bulk and right-localized modes, corresponding to the points marked in (b). (d) Variation of the finite plate spectrum in (b) as a function of μ_y . The red surface represents the dispersion of the edge state, while shaded gray volumes are the bulk bands. The red line at $\mu_y = 0$ highlights the transition of the edge state from left-localized (dashed) to right localized (solid) that occurs at $\phi = \pi$. (e) Steady-state response $|w(x, y)|$ of the modulated plate at frequency $\Omega = 10.97$, where the associated colormap also represents normalized displacement. Topological pumping occurs through a transition of the edge state from left-localized ($\phi_i = 0.5\pi$) to right localized ($\phi_f = 1.5\pi$) due to the phase modulation $\phi(y) = \phi_i \rightarrow \phi_f$. (c) Cross section of dispersion diagram in (d) at frequency $\Omega = 10.97$ as a function of $\phi \in [0.5\pi, 1.5\pi]$. Black and red lines respectively denote bulk and edge modes of the finite plate. The contours represent the spectrogram of the displacement field $|\hat{w}(y, \mu_y)|$, revealing that pumping occurs through a transition along the wavenumber branch of the edge state.

gray volumes) of Fig. 2(d), and represent the dispersion bands $\mu_y(\Omega = 10.97, \phi)$ occupied for $\mu_x \in \{0, \pi\}$. These bands are populated by modes of the finite plate with $L_x = 20\lambda_m$ (solid black lines), while the intersection between the blue plane and the red surface in Fig. 2(d) defines the edge state (red line) that spans the gap as a function of ϕ . The previously described forcing profile selectively excites the left-localized edge state (for $\phi_i = 0.5\pi$) at the bottom boundary of the plate, while a smooth phase modulation $\phi(y) = \phi_i \rightarrow \phi_f$ drives the left-to-right transition of the edge state along y , which occurs along the branch defined by the red lines in Fig. 2(f). We verify such transition by computing 2D Fourier Transforms (FT) while performing an appropriate windowing of the displacement field to capture wavenumber changes

along y . The procedure consists on pre-multiplying the displacement field $w(x, y)$ by a Gaussian window centered at $y = y_0$, *i.e.* $G(x, y) = e^{-(y-y_0)^2/2c^2}$, where c is a parameter controlling the Gaussian's width. A FT operation then quantifies the displacement field in reciprocal space $\hat{w}(y_0, \mu_x, \mu_y)$ around the location $y = y_0$. The dependence of μ_x is then eliminated by taking the L^1 norm along μ_x , which produces $\hat{w}(y, \mu_y)$. The corresponding spectrogram, obtained for $c = 0.07$, is displayed in the form of contour plots in Fig. 2(f), where the colors represent the normalized magnitude of the displacement field $|\hat{w}(y, \mu_y)|$. The procedure confirms that energy remains concentrated on the wavenumber branch of the edge state according to the modulation $\phi(y)$, which characterizes the topological pump displayed in Fig. 2(e).

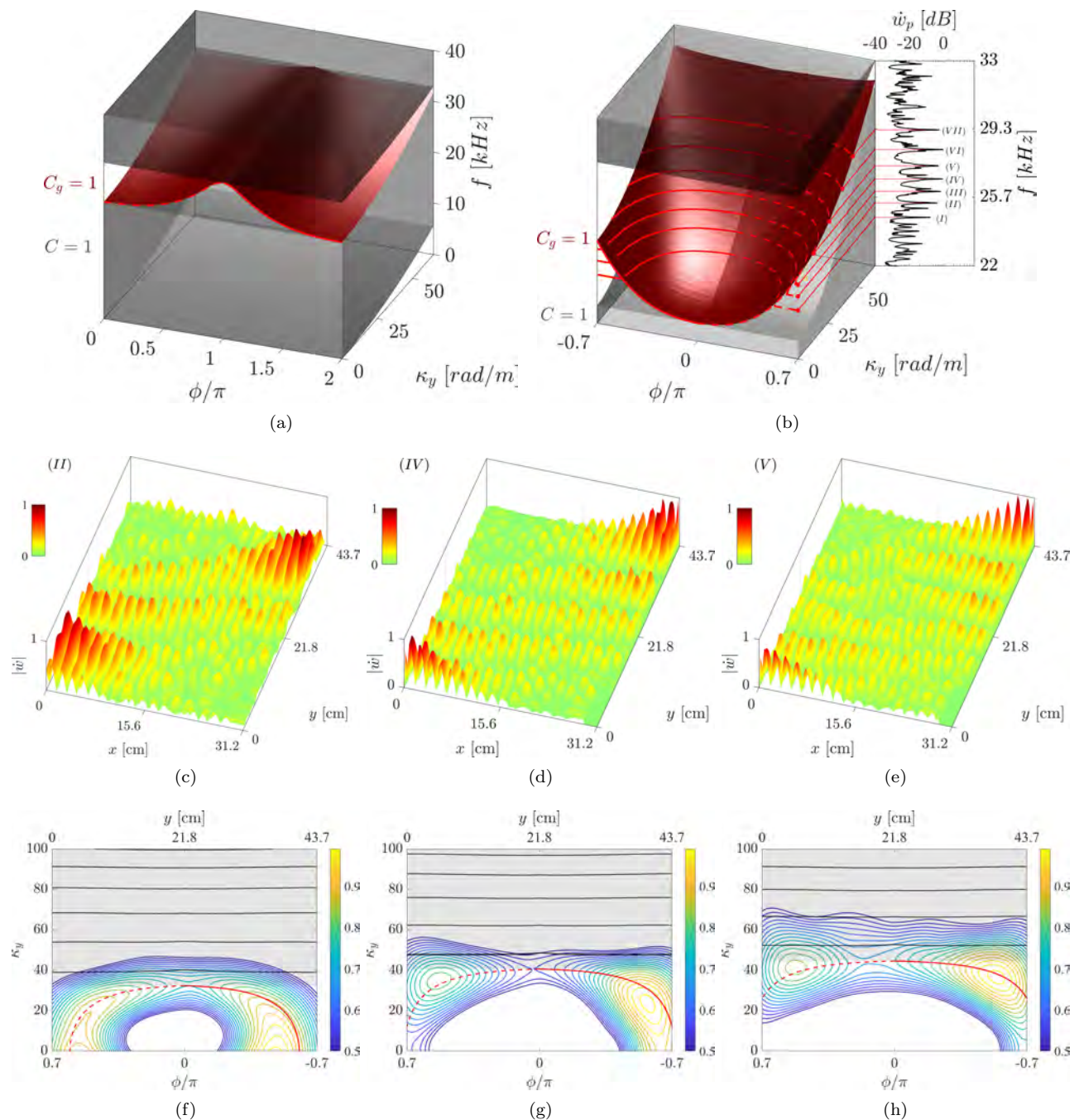


FIG. 3. Dispersion properties and experimental observation of topological pumping in plate with square-wave modulation of the thickness $h(x, y) = h_0[1 + a_m \text{sign}(\cos(\kappa_m x + \phi(y)))]$. (a) Dispersion properties and edge state (red surface) for a finite plate with $L_x = 31.2\text{cm}$ and free-free boundary conditions along x . Bulk bands are represented by shaded gray volumes, along with Chern number and gap labels information. (b) Detail of dispersion for $\phi \in [-0.7\pi, 0.7\pi]$, corresponding to the interval considered for the phase modulation of thickness. The experimentally measured frequency response spatially averaged over the plate surface is displayed alongside the dispersion. Each resonant peak defines a wavenumber branch highlighted by dashed and solid red lines in the dispersion surface, along which topological pumping occurs at the corresponding frequency. (c-e) Experimentally measured velocity field $|\dot{w}(x, y)|$ for selected resonant peaks II, IV and V. The transitions from localization at the left-boundary to localization at the right-boundary that characterize topological pumping are quantified by the spectrograms displayed in (f-h), which confirm that energy is concentrated around the wavenumber branches of the edge states.

III. EXPERIMENTAL OBSERVATION OF TOPOLOGICAL PUMPING IN SQUARE-MODULATED PLATE

Topological pumping is experimentally demonstrated in a plate with square-wave thickness modulation

$h(x, y) = h_0[1 + a_m \text{sign}(\cos(\kappa_m x + \phi(y)))]$ with modulation parameters $\lambda_m = 1.6\text{ cm}$, $h_0 = 4.7\text{ cm}$, $a_m = 0.38$,

$\phi_i = 0.7\pi$ and $\phi_f = -0.7\pi$ (Fig. 1(b)). The plate is rectangular of dimensions $31.2 \text{ cm} \times 43.7 \text{ cm}$, and it is made of aluminum (Fig. 1(d)). A linear phase modulation produces the tilted thickness profile in Fig. 1(d).

The plate dispersion properties are computed using a Finite Element (FE) model implemented in the COMSOL Multiphysics environment⁴⁶. The computations provide information on all wave modes, whose polarizations are tracked by computing a polarization factor²⁰ that quantifies the relationship between in-plane (u, v) and out-of-plane (w) components of the displacement field. The polarization factor is employed to discriminate and isolate out-of-plane polarized wave modes, which are weakly coupled to the in-plane ones. We compare the results to experimental data consisting of the out-of-plane velocity field $\dot{w}(x, y, t)$ of the plate's surface measured by a scanning laser Doppler vibrometer (SLDV) (see details in SM⁴⁶).

The numerically computed dispersion relations are shown in Fig. 3(a), where, as previously, the red surface corresponds to the edge state, while the shaded gray volumes denote the bulk bands. Similar to the case of harmonic modulation, the existence of an edge state spanning the gap is associated with the non-trivial band topology identified by integer-valued Chern numbers. Chern numbers and gap labels are numerically evaluated using the Bloch modes obtained through the FE model according to the procedure outlined in SM⁴⁶, which yields the labels displayed in Fig. 3(a). We find that the first spectral gap produced by the square modulation is also characterized by a gap label $C_g = 1$, which signals a left to right transition of the edge state, again highlighted by the dashed and solid red lines at $\kappa_y = 0$. This transition occurs at $\phi = \pi$ along the entire surface of the edge state, which is consistent with constant valued Chern numbers evaluated as a function of κ_y in the considered frequency range ($f \in [0, 40]$ kHz). Figure 3(b) displays a zoomed view of the dispersion in Fig. 3(a) for $\phi \in [-0.7\pi, 0.7\pi]$, with the observation that the interval $[-0.7\pi, 0]$ coincides with $[1.3\pi, 2\pi]$ due to the periodicity with ϕ . This interval corresponds to the phase modulation of the manufactured plate, *i.e.* from $\phi_i = 0.7\pi$ to $\phi_f = -0.7\pi$, which exhibits the transition of the edge state occurring at the bottom boundary of the gap.

The experiment is conducted by clamping the plate at its bottom right boundary while excitation is induced by a pair of piezoelectric ceramic patches attached to the bottom left boundary⁴⁶. The patches are connected to opposite electrical poles, which induces an out-of-phase (dipole) excitation that favors the excitation of the left-localized topological mode (for $\phi_i = 0.7\pi$), while reducing the contribution from bulk modes. The forced frequency response function, corresponding to the response spatially averaged over the plate surface, is displayed alongside the dispersion surfaces. The finite size of the plate introduces a series of resonant peaks that are observed in the frequency range within which the edge state exists. At these frequencies, topological pumping is ob-

served through a transition along the wavenumber branch of the edge state, as illustrated by the dashed and solid red lines in Fig. 3(b), respectively denoting left and right localized modes. The measured velocity fields for three selected resonant frequencies are displayed in Figs. 3(c-e), where transitions from left to right localization characterizing the pump can be observed. For each of those recorded responses, a spectrogram is computed as described in Section II and displayed in Figs. 3(f-h), which confirms the transition along the wavenumber branch corresponding to the edge state. We remark that for the first peaks, such as in the case reported in Fig. 3(c), the edge state is only defined within a restricted domain of the parameter space. In such cases, pumping still occurs through the wavenumber branch of the edge state, but is defined in a shorter spatial domain centered at the mid-portion of the plate, as confirmed by the spectrogram of Fig. 3(f) corresponding to the pump of peak *II*.

The results reported in Fig. 3 confirm the existence of steady-state topological pumping in the square-modulated plate occurring for several operating frequencies within $[25, 30]$ kHz, while populating the dispersion surface associated with the edge state. The potential of the modulated plate as a waveguiding platform is further demonstrated by realizing topological pumping in a transient regime. To that end, an excitation in the form of a 7-cycle sine burst signal of center frequency $f = 26.7$ kHz is employed, which aims at transporting energy through the pump defined by peak *IV* in Fig. 3(b). Figure 4 displays the measured velocity wavefield in the modulated plate at three subsequent time instants: a clear transition from left-localized wave (a), to bulk wave (b), and finally to right-localized wave propagation (c) is observed consistent with the expected topological pumping behavior. A video animation of the full transient response is provided in SM⁴⁶.

IV. CONCLUSIONS

In this paper, we present the first experimental demonstration of topological pumping in continuous elastic plates. We illustrate a simple design principle based on continuous property modulations which can be employed to induce the existence of topological edge states and drive their edge-to-edge transition. The results also provide opportunities for exploring higher dimensional physics in mechanics by exploiting synthetic dimensions in parameter space, which can be mapped to real spatial or temporal dimensions. These concepts have implications of technological relevance for applications involving elastic wave manipulation, such as guiding of bulk, surface and guided waves in acoustic devices, ultrasonic imaging and nondestructive evaluation.

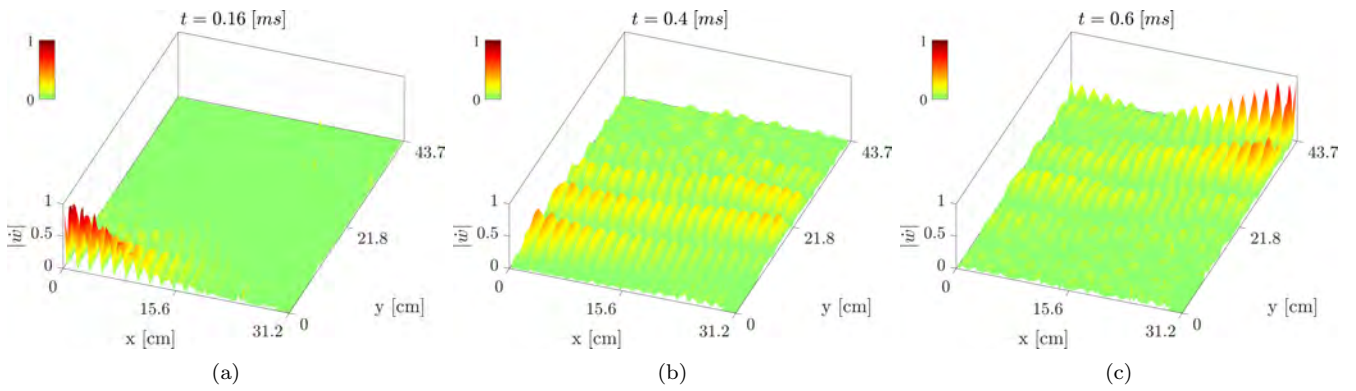


FIG. 4. Experimental observation of transient topological pumping in square-modulated plate. Figures (a-c) displays snapshots of the measured velocity field for three subsequent time instants, where the transition from left-localized (a), to bulk (b), and finally to right localized mode (c) as the wave propagates along y can be observed.

ACKNOWLEDGMENTS

The authors gratefully acknowledge the support from the National Science Foundation (NSF) through the

EFRI 1741685 grant and from the Army Research office through grant W911NF-18-1-0036.

-
- ¹ M Zahid Hasan and Charles L Kane. Colloquium: topological insulators. *Reviews of Modern Physics*, 82(4):3045, 2010.
 - ² Ling Lu, John D Joannopoulos, and Marin Soljačić. Topological photonics. *Nature Photonics*, 8(11):821, 2014.
 - ³ Alexander B Khanikaev, S Hossein Mousavi, Wang-Kong Tse, Mehdi Kargarian, Allan H MacDonald, and Gennady Shvets. Photonic topological insulators. *Nature materials*, 12(3):233, 2013.
 - ⁴ Zhaoju Yang, Fei Gao, Xihang Shi, Xiao Lin, Zhen Gao, Yidong Chong, and Baile Zhang. Topological acoustics. *Phys. Rev. Lett.*, 114:114301, Mar 2015.
 - ⁵ Romain Fleury, Alexander B Khanikaev, and Andrea Alu. Floquet topological insulators for sound. *Nature communications*, 7:11744, 2016.
 - ⁶ Jiuyang Lu, Chunyin Qiu, Liping Ye, Xiyang Fan, Manzhou Ke, Fan Zhang, and Zhengyou Liu. Observation of topological valley transport of sound in sonic crystals. *Nature Physics*, 13(4):369, 2017.
 - ⁷ S Hossein Mousavi, Alexander B Khanikaev, and Zheng Wang. Topologically protected elastic waves in phononic metamaterials. *Nature communications*, 6:8682, 2015.
 - ⁸ K v Klitzing, Gerhard Dorda, and Michael Pepper. New method for high-accuracy determination of the fine-structure constant based on quantized hall resistance. *Physical Review Letters*, 45(6):494, 1980.
 - ⁹ David J Thouless, Mahito Kohmoto, M Peter Nightingale, and Md den Nijs. Quantized hall conductance in a two-dimensional periodic potential. *Physical review letters*, 49(6):405, 1982.
 - ¹⁰ Emil Prodan and Camelia Prodan. Topological phonon modes and their role in dynamic instability of microtubules. *Physical review letters*, 103(24):248101, 2009.
 - ¹¹ Pai Wang, Ling Lu, and Katia Bertoldi. Topological phononic crystals with one-way elastic edge waves. *Physical review letters*, 115(10):104302, 2015.
 - ¹² Lisa M Nash, Dustin Kleckner, Alismari Read, Vincenzo Vitelli, Ari M Turner, and William TM Irvine. Topological mechanics of gyroscopic metamaterials. *Proceedings of the National Academy of Sciences*, 112(47):14495–14500, 2015.
 - ¹³ Anton Souslov, Benjamin C Van Zuiden, Denis Bartolo, and Vincenzo Vitelli. Topological sound in active-liquid metamaterials. *Nature Physics*, 13(11):1091, 2017.
 - ¹⁴ Noah P Mitchell, Lisa M Nash, Daniel Hexner, Ari M Turner, and William TM Irvine. Amorphous topological insulators constructed from random point sets. *Nature Physics*, 14(4):380, 2018.
 - ¹⁵ H Chen, LY Yao, H Nassar, and GL Huang. Mechanical quantum hall effect in time-modulated elastic materials. *Physical Review Applied*, 11(4):044029, 2019.
 - ¹⁶ Roman Süssstrunk and Sebastian D Huber. Observation of phononic helical edge states in a mechanical topological insulator. *Science*, 349(6243):47–50, 2015.
 - ¹⁷ Raj Kumar Pal, Marshall Schaeffer, and Massimo Ruzzene. Helical edge states and topological phase transitions in phononic systems using bi-layered lattices. *Journal of Applied Physics*, 119(8):084305, 2016.
 - ¹⁸ H. Chen, H. Nassar, A. N. Norris, G. K. Hu, and G. L. Huang. Elastic quantum spin hall effect in kagome lattices. *Phys. Rev. B*, 98:094302, Sep 2018.
 - ¹⁹ Rajesh Chaunsali, Chun-Wei Chen, and Jinkyu Yang. Sub-wavelength and directional control of flexural waves in zone-folding induced topological plates. *Physical Review B*, 97(5):054307, 2018.
 - ²⁰ M. Miniaci, R. K. Pal, B. Morvan, and M. Ruzzene. Experimental observation of topologically protected helical edge modes in patterned elastic plates. *Phys. Rev. X*, 8:031074, Sep 2018.
 - ²¹ Raj Kumar Pal and Massimo Ruzzene. Edge waves in plates with resonators: an elastic analogue of the quantum

- valley hall effect. *New Journal of Physics*, 19(2):025001, 2017.
- ²² Javier Vila, Raj Kumar Pal, and Massimo Ruzzene. Observation of topological valley modes in an elastic hexagonal lattice. *Physical Review B*, 96(13):134307, 2017.
- ²³ Ting-Wei Liu and Fabio Semperlotti. Tunable acoustic valley–hall edge states in reconfigurable phononic elastic waveguides. *Physical Review Applied*, 9(1):014001, 2018.
- ²⁴ Ting-Wei Liu and Fabio Semperlotti. Experimental evidence of robust acoustic valley hall edge states in a non-resonant topological elastic waveguide. *Physical Review Applied*, 11(1):014040, 2019.
- ²⁵ Xiao-Liang Qi, Taylor L Hughes, and Shou-Cheng Zhang. Topological field theory of time-reversal invariant insulators. *Physical Review B*, 78(19):195424, 2008.
- ²⁶ Yaacov E Kraus and Oded Zilberberg. Quasiperiodicity and topology transcend dimensions. *Nature Physics*, 12(7):624, 2016.
- ²⁷ Tomoki Ozawa, Hannah M Price, Nathan Goldman, Oded Zilberberg, and Iacopo Carusotto. Synthetic dimensions in integrated photonics: From optical isolation to four-dimensional quantum hall physics. *Physical Review A*, 93(4):043827, 2016.
- ²⁸ Ching Hua Lee, Yuzhu Wang, Youjian Chen, and Xiao Zhang. Electromagnetic response of quantum hall systems in dimensions five and six and beyond. *Physical Review B*, 98(9):094434, 2018.
- ²⁹ VM Martinez Alvarez and MD Coutinho-Filho. Edge states in trimer lattices. *Physical Review A*, 99(1):013833, 2019.
- ³⁰ Yaacov E Kraus, Yoav Lahini, Zohar Ringel, Mor Verbin, and Oded Zilberberg. Topological states and adiabatic pumping in quasicrystals. *Physical review letters*, 109(10):106402, 2012.
- ³¹ David J Apigo, Wenting Cheng, Kyle F Dobiszewski, Emil Prodan, and Camelia Prodan. Observation of topological edge modes in a quasiperiodic acoustic waveguide. *Physical review letters*, 122(9):095501, 2019.
- ³² Xiang Ni, Kai Chen, Matthew Weiner, David J Apigo, Camelia Prodan, Andrea Alù, Emil Prodan, and Alexander B Khanikaev. Observation of hofstadter butterfly and topological edge states in reconfigurable quasi-periodic acoustic crystals. *Communications Physics*, 2(1):55, 2019.
- ³³ David J Apigo, Kai Qian, Camelia Prodan, and Emil Prodan. Topological edge modes by smart patterning. *Physical Review Materials*, 2(12):124203, 2018.
- ³⁴ Matheus IN Rosa, Raj Kumar Pal, José RF Arruda, and Massimo Ruzzene. Edge states and topological pumping in spatially modulated elastic lattices. *Physical Review Letters*, 123(3):034301, 2019.
- ³⁵ Raj Kumar Pal, Matheus I N Rosa, and Massimo Ruzzene. Topological bands and localized vibration modes in quasiperiodic beams. *New Journal of Physics*, 21(9):093017, sep 2019.
- ³⁶ Philip George Harper. Single band motion of conduction electrons in a uniform magnetic field. *Proceedings of the Physical Society. Section A*, 68(10):874, 1955.
- ³⁷ Serge Aubry and Gilles André. Analyticity breaking and anderson localization in incommensurate lattices. *Ann. Israel Phys. Soc*, 3(133):18, 1980.
- ³⁸ Oded Zilberberg, Sheng Huang, Jonathan Guglielmon, Mohan Wang, Kevin P Chen, Yaacov E Kraus, and Mikael C Rechtsman. Photonic topological boundary pumping as a probe of 4d quantum hall physics. *Nature*, 553(7686):59, 2018.
- ³⁹ Michael Lohse, Christian Schweizer, Hannah M Price, Oded Zilberberg, and Immanuel Bloch. Exploring 4d quantum hall physics with a 2d topological charge pump. *Nature*, 553(7686):55, 2018.
- ⁴⁰ Ioannis Petrides, Hannah M Price, and Oded Zilberberg. Six-dimensional quantum hall effect and three-dimensional topological pumps. *Physical Review B*, 98(12):125431, 2018.
- ⁴¹ Mor Verbin, Oded Zilberberg, Yoav Lahini, Yaacov E Kraus, and Yaron Silberberg. Topological pumping over a photonic fibonacci quasicrystal. *Physical Review B*, 91(6):064201, 2015.
- ⁴² Shuta Nakajima, Takafumi Tomita, Shintaro Taie, Tomohiro Ichinose, Hideki Ozawa, Lei Wang, Matthias Troyer, and Yoshiro Takahashi. Topological thouless pumping of ultracold fermions. *Nature Physics*, 12(4):296, 2016.
- ⁴³ Michael Lohse, Christian Schweizer, Oded Zilberberg, Monika Aidelsburger, and Immanuel Bloch. A thouless quantum pump with ultracold bosonic atoms in an optical superlattice. *Nature Physics*, 12(4):350, 2016.
- ⁴⁴ Inbar Hotzen Grinberg, Mao Lin, Cameron Harris, Wladimir A Benalcazar, Christopher W Peterson, Taylor L Hughes, and Gaurav Bahl. Robust temporal pumping in a magneto-mechanical topological insulator. *arXiv preprint arXiv:1905.02778*, 2019.
- ⁴⁵ Karl F Graff. *Wave motion in elastic solids*. Courier Corporation, 2012.
- ⁴⁶ See supplemental material at xxxx for more details on the simulation procedures, experimental setup and methodology, and for a video animation of the transient experimental analysis.
- ⁴⁷ L Meirovitch. *Elements of vibration analysis*. McGraw-Hill, 1975.
- ⁴⁸ Yasuhiro Hatsugai. Chern number and edge states in the integer quantum hall effect. *Physical review letters*, 71(22):3697, 1993.
- ⁴⁹ Takahiro Fukui, Yasuhiro Hatsugai, and Hiroshi Suzuki. Chern numbers in discretized brillouin zone: efficient method of computing (spin) hall conductances. *Journal of the Physical Society of Japan*, 74(6):1674–1677, 2005.
- ⁵⁰ H Nassar, H Chen, AN Norris, and GL Huang. Quantization of band tilting in modulated phononic crystals. *Physical Review B*, 97(1):014305, 2018.